《高阶会员专属视频》
-第31期

IEEE论文导读：稳定的永磁同步电机Sensorless开环VF控制技术

《高階會員專屬-第31期》IEEE論文導讀：穩定的永磁同步電機Sensorless開回路VF控制技術

IEEE TRANSACTIONS ON INDUSTRY APPLICATIONS, VOL. 39, NO. 3, MAY/JUNE 2003

A Sensorless, Stable V/f Control Method for Permanent-Magnet Synchronous Motor Drives

P. D. Chandana Perera, *Student Member, IEEE*, Frede Blaabjerg, *Fellow, IEEE*,
John K. Pedersen, *Senior Member, IEEE*, and Paul Thøgersen, *Senior Member, IEEE*

《高階會員專屬-第31期》IEEE論文導讀：穩定的永磁同步電機Sensorless開回路VF控制技術

***Abstract*—When permanent-magnet synchronous motors (PMSMs) are used for pump and fan applications, V/f control methods can be used to control them. The problem with open-loop V/f control of PMSMs without having damper windings in the rotor is the inherent instability after exceeding a certain applied frequency. In this paper, a new V/f control method is proposed for motor drives for stable operation in a wide frequency range. The magnitude of the voltage is controlled in order to maintain a constant stator flux linkage in the PMSM. The applied frequency is modulated proportional to the input power perturbations to stabilize the drive for a wide frequency range. No position sensor is required to implement this stabilizing technique. The small-signal analysis and the experimental results confirm the effectiveness of this stabilizing technique. The experimental results also indicate the satisfactory performance of the drive for pump and fan applications.**

《高階會員專屬-第31期》IEEE論文導讀：穩定的永磁同步電機Sensorless開回路VF控制技術

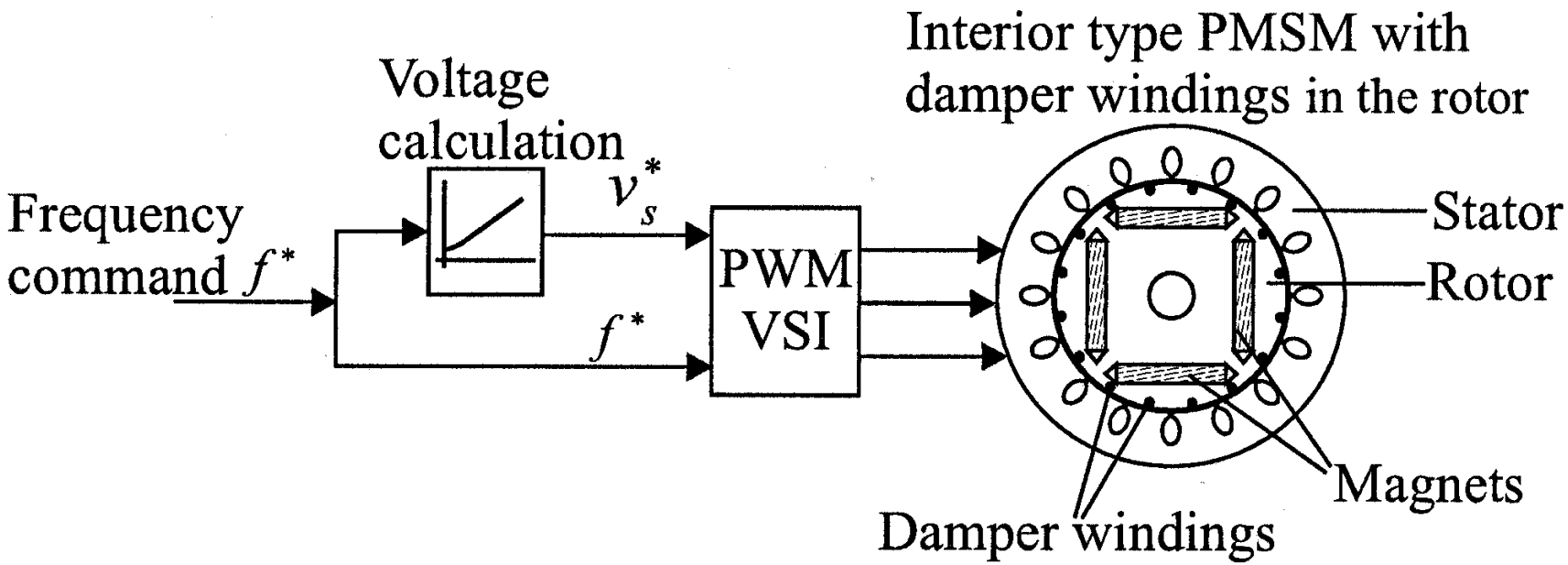

Fig. 1. Open-loop V/f control approach, which can be used for interior-type PMSMs with damper windings in the rotor.

《高階會員專屬-第31期》IEEE論文導讀：穩定的永磁同步電機Sensorless開回路VF控制技術

Due to the high manufacturing cost and the difficulty to design rotors with damper windings for some type of PMSMs (e.g., surface-mounted-type PMSMs), the PMSMs are not generally available with damper windings in the rotor. The PMSMs without damper windings in the rotor do not assure the synchronization of motion of the rotor with stator applied frequency under the open-loop V/f control approach shown in Fig. 1. This causes instability problems in those PMSMs under the open-loop V/f control approach and an additional signal is required to the V/f controller in order to assure the synchronization and the stable operation.

《高階會員專屬-第31期》IEEE論文導讀：穩定的永磁同步電機Sensorless開回路VF控制技術

A stable i/f control method was proposed in [11] for a synchronous reluctance motor without damper windings in the rotor. The current control provides overcurrent protection and better starting performance in this drive compared to the V/f control approach. The stabilization of the drive was achieved by adjusting the current amplitude according to the power-factor angle variation. However, there was no analytical model given to design this i/f controller.

《高階會員專屬-第31期》IEEE論文導讀：穩定的永磁同步電機Sensorless開回路VF控制技術

In this paper, a new V/f control method incorporating a stabilizing technique is proposed for the PMSMs without damper windings in the rotor. A voltage control method in order to improve to the low-speed performance of the drive is first discussed, followed by the stability analysis of the drive. This leads to the discussion on stabilization of the drive. Using small-signal model analysis it will be shown that modulating the applied frequency proportional to the input power perturbations can add necessary damping and stabilize the drive for a wide frequency range operation. This is followed by experimental results to validate the control strategy.

《高階會員專屬-第31期》IEEE論文導讀：穩定的永磁同步電機Sensorless開回路VF控制技術

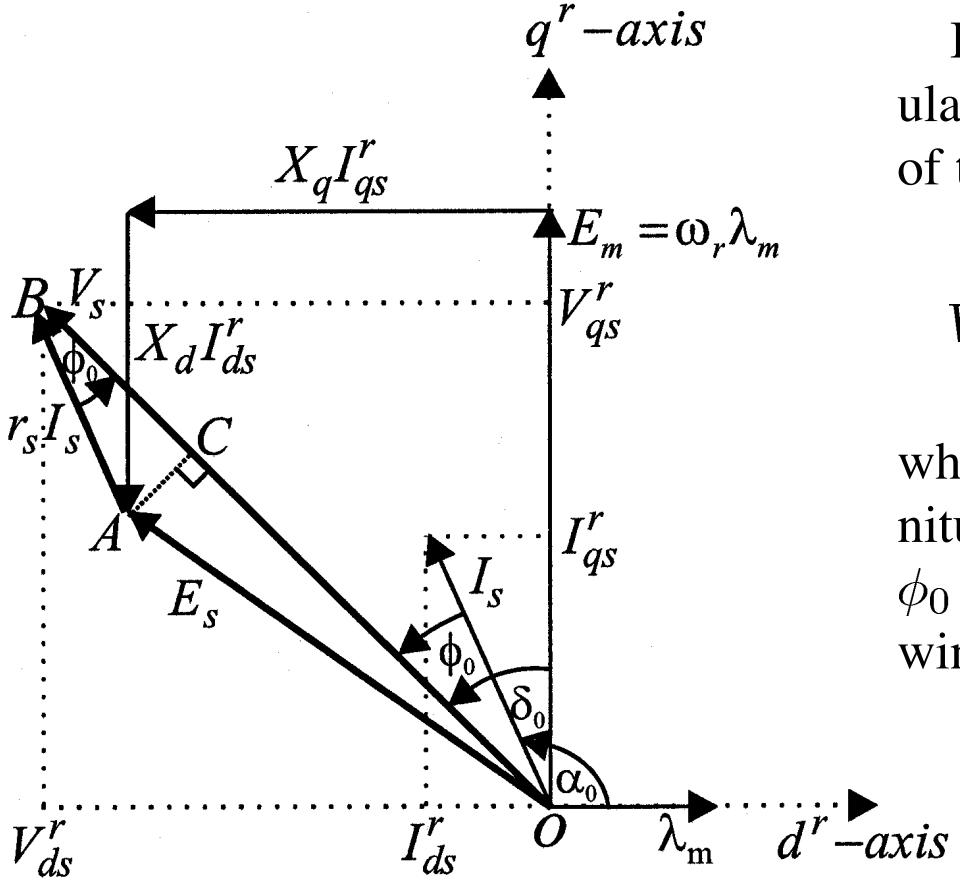

In the triangle *OAB* shown in Fig. 2, *AC* is drawn perpendicular to *OB*. From the *OAB* triangle the steady-state magnitude of the voltage vector V_s can be obtained as

$$V_s = BC + CO = I_s r_s \cos\phi_0 + \sqrt{E_s^2 - I_s^2 r_s^2 \sin^2\phi_0} \quad (1)$$

where I_s is the magnitude of the current vector, E_s is the magnitude of the voltage vector induced by stator flux linkage, and ϕ_0 is the power factor angle; all are in steady state. r_s is stator winding resistance per phase.

Fig. 2. Steady-state vector diagram of the PMSM showing the stator voltage vector as an addition of stator resistance voltage drop and induced voltage from the stator flux (in the triangle *OAB*).

《高階會員專屬-第31期》IEEE論文導讀：穩定的永磁同步電機Sensorless開回路VF控制技術

Using the trigonometric relationship $\sin^2\phi_0 + \cos^2\phi_0 = 1$, the magnitude of the voltage vector obtained in (1) can also be written as

$$V_s = I_s r_s \cos\phi_0 + \sqrt{E_s^2 + I_s^2 r_s^2 \cos^2\phi_0 - I_s^2 r_s^2}. \quad (2)$$

Equation (2) can be used to calculate the magnitude of the voltage command to the PMSM. The stator-flux-induced voltage E_s in (2), can be calculated from the required steady-state constant stator flux. The constant magnitude of the stator flux vector is selected as the rotor permanent-magnet flux λ_m. With this selection, the stator voltage requirement to the machine can be kept comparably low and the no-load current of the machine can be minimized. With this selection of the magnitude of the stator flux, E_s can be calculated as

$$E_s = 2\pi f_0 \lambda_m \quad (3)$$

where f_0 is the applied frequency to the machine.

《高階會員專屬-第31期》IEEE論文導讀：穩定的永磁同步電機Sensorless開回路VF控制技術

Even though I_s and $\cos\phi_0$ are steady-state values, the instantaneously measured values of them can be used in (2) to command the magnitude of the voltage, so that the steady-state induced voltage from the stator flux will be the value given in (3). The term $I_s \cos\phi_0$ in (2) is the stator current vector component along with the stator voltage vector. By transforming the measured phase currents to the stator voltage fixed reference frame this term can instantaneously be calculated as

$$i_s \cos\phi = \frac{2}{3}\left[i_{as}\cos\theta_e + i_{bs}\cos\left(\theta_e - \frac{2\pi}{3}\right) - (i_{as}+i_{bs})\cos\left(\theta_e + \frac{2\pi}{3}\right)\right] \quad (4)$$

where i_s and ϕ are the instantaneous values of magnitude of the current vector and the power-factor angle, respectively. i_{as}, i_{bs} are measured phase currents and θ_e is the position of the voltage vector in the stationary reference frame.

《高階會員專屬-第31期》IEEE論文導讀：穩定的永磁同步電機Sensorless開回路VF控制技術

i_s can also be obtained by measuring two phase currents and calculating the stationary d^s, q^s reference frame current components as given in (5)

$$i_s = \sqrt{(i_{ds}^s)^2 + (i_{qs}^s)^2} = \sqrt{\frac{1}{3}(i_{as} + 2i_{bs})^2 + (i_{as})^2}. \quad (5)$$

For both (4) and (5), the reference frame transformation equations described in [13] are used.

《高階會員專屬-第31期》IEEE論文導讀：穩定的永磁同步電機Sensorless開回路VF控制技術

Using the instantaneously calculated values and the commanded value for E_s the final expression for calculation of magnitude of the voltage command v_s^* can be written as

$$v_s^* = (i_s \cos\phi) r_s + \sqrt{(2\pi f_0 \lambda_m)^2 + (i_s \cos\phi)^2 r_s^2 - i_s^2 r_s^2}. \tag{6}$$

Measuring the instantaneous currents the implementation of (6) in the drive system is shown in Fig. 3. To eliminate the high-frequency ripples in the calculated currents i_s and $i_s \cos\phi$, two low-pass filters (LPFs) are used as shown in Fig. 3.

《高階會員專屬-第31期》IEEE論文導讀：穩定的永磁同步電機Sensorless開回路VF控制技術

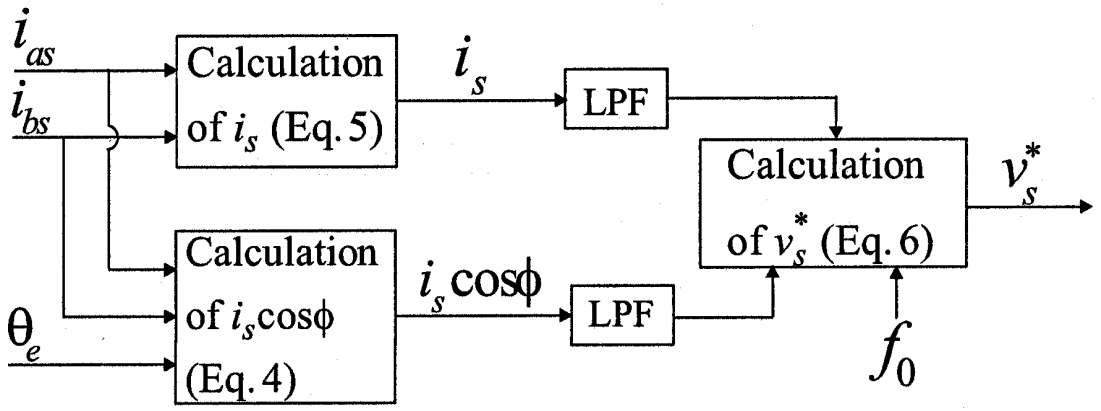

Fig. 3. Calculation of the voltage command.

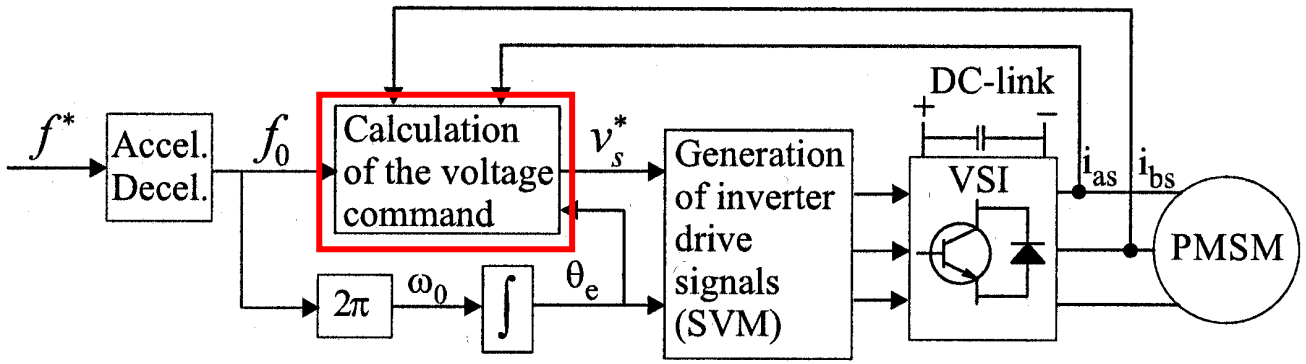

Fig. 4. Preliminary drive configuration with voltage control method.

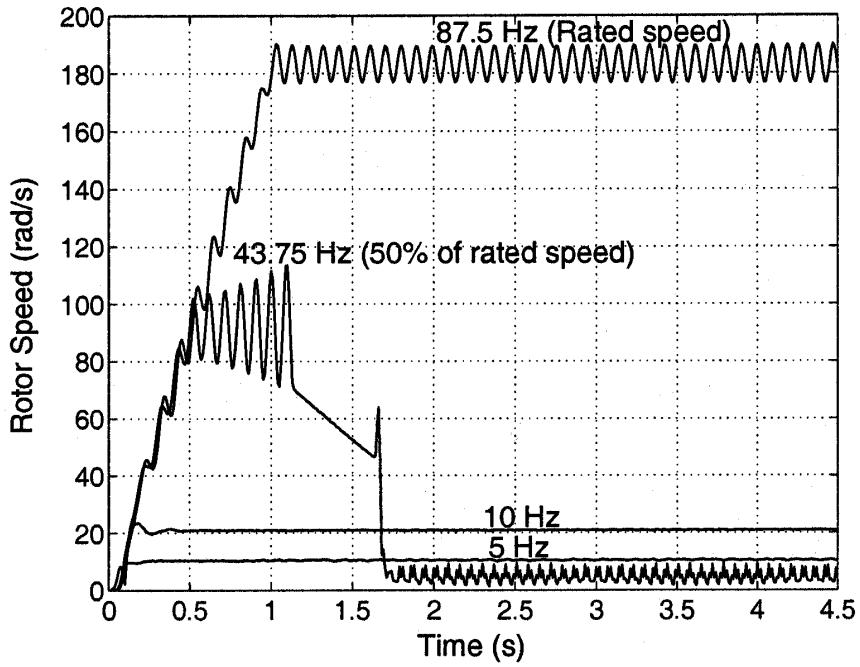

Fig. 13. Measured rotor speeds at different frequencies, under no load, without stabilizing loop in the system.

《高階會員專屬-第31期》IEEE論文導讀：穩定的永磁同步電機Sensorless開回路VF控制技術

B. Stability Analysis

To analyze the stability of the PMSM under constant stator flux linkage control, the linearized PMSM model is used. The eigenvalues of the state transition matrix of the linearized PMSM model should show the stability behavior of the PMSM for the conditions under consideration [15], [16].

The state variable form of the rotor d^r, q^r frame equations of the PMSM without having damper windings in the rotor can be written as

$$pi_{qs}^r = \frac{-i_{qs}^r}{\sigma\tau_s} - \frac{\omega_r}{\sigma}\left(\frac{\lambda_m}{L_d} + i_{ds}^r\right) + \frac{v_s\cos(\delta)}{\sigma L_d} \tag{7}$$

$$pi_{ds}^r = \frac{-i_{ds}^r}{\tau_s} + \sigma\omega_r i_{qs}^r - \frac{v_s\sin(\delta)}{L_d} \tag{8}$$

$$p\omega_r = \frac{3}{2J}\left(\frac{n}{2}\right)^2[\lambda_m i_{qs}^r + L_d(1-\sigma)i_{qs}^r i_{ds}^r] - \frac{1}{J}B_m\omega_r - \frac{n}{2J}T_l \tag{9}$$

$$p\delta = \omega_e - \omega_r. \tag{10}$$

In (7)–(10),

$\tau_s = L_d/r_s$, $\sigma = L_q/L_d$;

i_{qs}^r, i_{ds}^r rotor q^r- and d^r-axes currents;
L_q, L_d rotor q^r- and d^r-axes inductances;
p operator d/dt;
ω_r electrical rotor speed;
ω_e electrical speed of the applied voltage vector;
δ load angle;
J inertia of the motor and the load system;
B_m viscous friction coefficient;
n number of poles of the motor;
T_l load torque.

《高階會員專屬-第31期》IEEE論文導讀：穩定的永磁同步電機Sensorless開回路VF控制技術

The machine state equations (7)–(10) have the form

$$\dot{x} = f(x, u) \tag{11}$$

where x is the vector of the machine state variables and f is the nonlinear function of the state x and the inputs u. The linearized system equations of this nonlinear system have the form

$$\dot{\Delta x} = A(X)\Delta x + B(X)\Delta u \tag{12}$$

where Δx is the perturbations matrix for state variables x, $A(X)$ is the state transition matrix, Δu is the input perturbation matrix, and $B(X)$ is the input matrix [16]. The derivation of the linearized machine equations is well discussed in [15] and [16]. The obtained linearized PMSM model can be written as in the matrix equation (13), shown at the bottom of the next page, which has the form given in (12). In (13), I_{qs}^r, I_{ds}^r, V_s, ω_0, and δ_0 represent the steady-state value of corresponding variable. When deriving this model, it is considered that the input voltage and the frequency to the PMSM are constant steady-state values, i.e., perturbations $\Delta v_s = 0$ and $\Delta \omega_e = 0$.

《高階會員專屬-第31期》IEEE論文導讀：穩定的永磁同步電機Sensorless開回路VF控制技術

$$p\begin{bmatrix}\Delta i_{qs}^{r}\\ \Delta i_{ds}^{r}\\ \Delta\omega_{r}\\ \Delta\delta\end{bmatrix}=\underbrace{\begin{bmatrix}\frac{-1}{\sigma\tau_s} & \frac{-\omega_0}{\sigma} & \frac{-1}{\sigma}\left(\frac{\lambda_m}{L_d}+I_{ds}^{r}\right) & \frac{-V_s}{\sigma L_d}\sin(\delta_0)\\ \sigma\omega_0 & \frac{-1}{\tau_s} & \sigma I_{qs}^{r} & \frac{-V_s}{L_d}\cos(\delta_0)\\ \frac{3}{2}\left(\frac{n}{2}\right)^2\frac{1}{J}[\lambda_m+L_d(1-\sigma)I_{ds}^{r}] & \frac{3}{2}\left(\frac{n}{2}\right)^2\frac{1}{J}L_d(1-\sigma)I_{qs}^{r} & \frac{-B_m}{J} & 0\\ 0 & 0 & -1 & 0\end{bmatrix}}_{A(X)}\begin{bmatrix}\Delta i_{qs}^{r}\\ \Delta i_{ds}^{r}\\ \Delta\omega_{r}\\ \Delta\delta\end{bmatrix}+\begin{bmatrix}0\\ 0\\ \frac{-n}{2J}\\ 0\end{bmatrix}\Delta T_l \tag{13}$$

《高階會員專屬-第31期》IEEE論文導讀：穩定的永磁同步電機Sensorless開回路VF控制技術

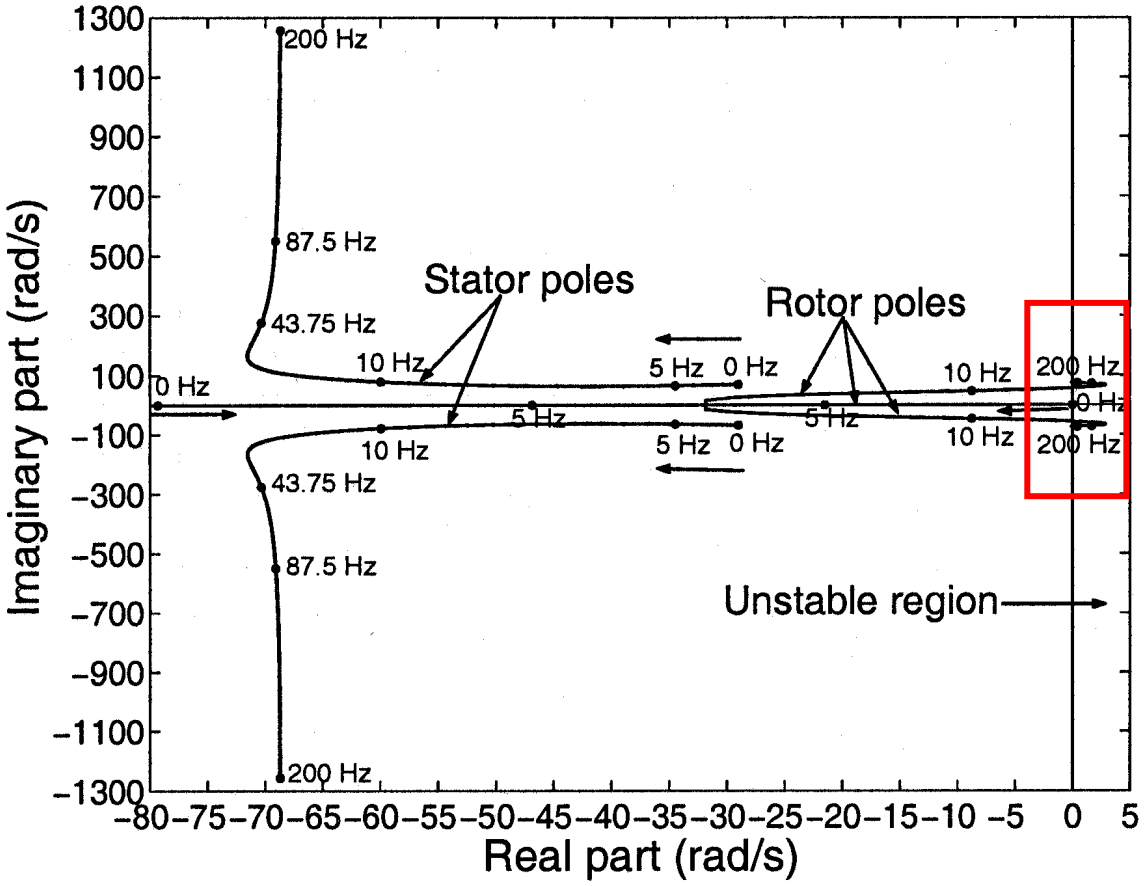

Fig. 5. Eigenvalue plot under no load, as a function of the applied frequency.

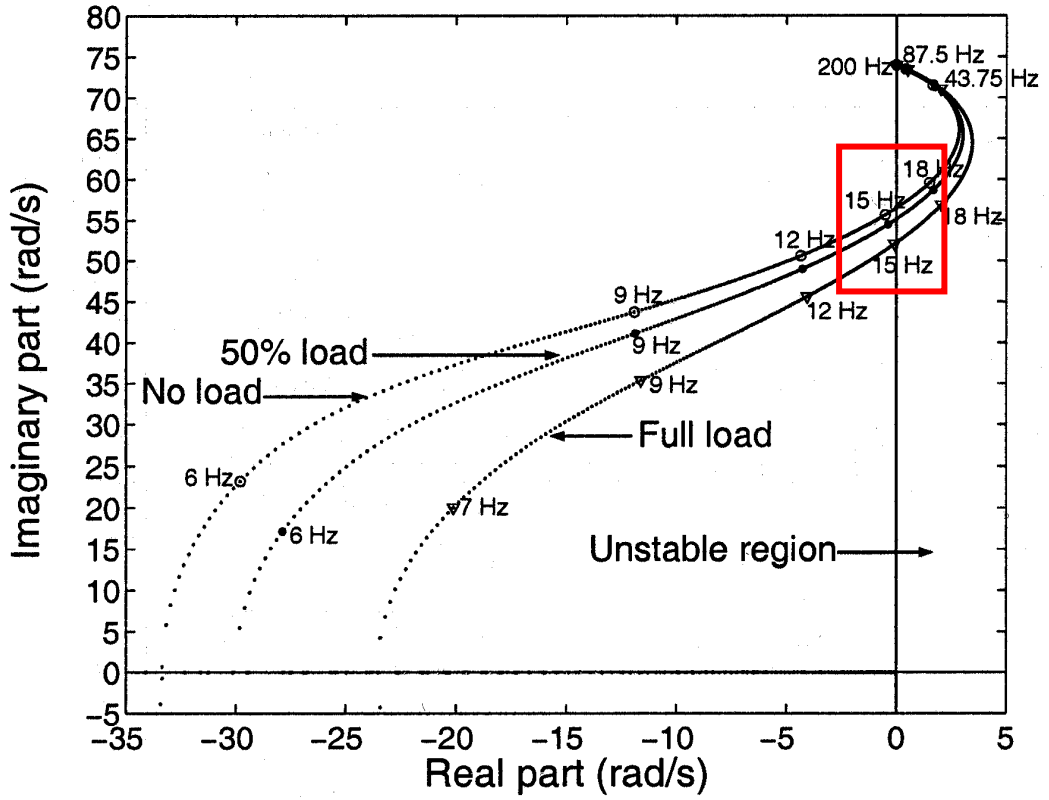

Fig. 6. Loci of the rotor poles under different load conditions, as a function of the applied frequency.

《高階會員專屬-第31期》IEEE論文導讀：穩定的永磁同步電機Sensorless開回路VF控制技術

III. Stabilization of the Drive by Frequency Modulation

The PMSM's instability behavior after exceeding a certain applied frequency observed in Section II-B is due to the nonexistence of rotor circuits (i.e., damper windings) and, therefore, the weak coupling between electrical and mechanical modes of the machine. The stator and rotor poles move away from each other and, after exceeding a certain applied frequency, the slow rotor poles cross over to the instability region of the s plane, having a small positive real part. To stabilize the system for the

《高階會員專屬-第31期》IEEE論文導讀：穩定的永磁同步電機Sensorless開回路VF控制技術

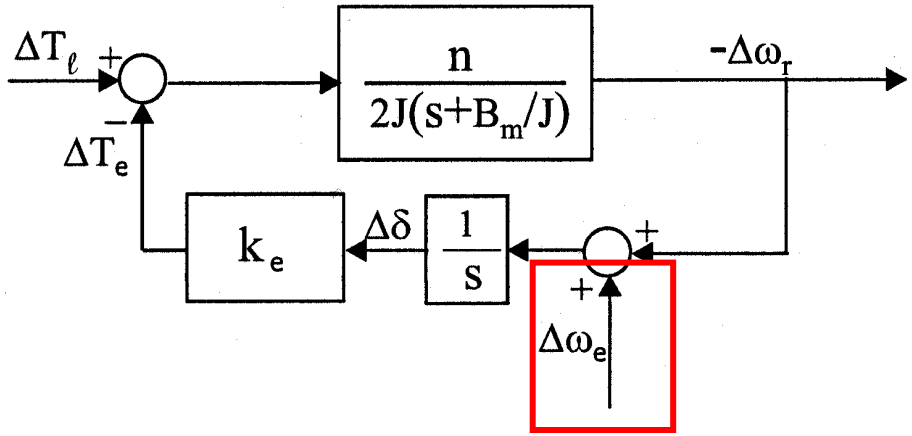

Fig. 7. Block diagram representation of the simplified small-signal dynamic model, which models only the rotor poles of the PMSM.

A. Simplified Small-Signal Dynamics Model Analysis

The insight of frequency modulation to add damping can be obtained from a simplified linearized model (simplified small-signal dynamics model) of the PMSM, which models only the rotor poles of the machine. This model in block diagram form is shown in Fig. 7. More details of this model can be found in [8] and [10].

The parameter k_e in Fig. 7 is the electromechanical spring constant and it is equal to the slope of the load-angle torque (δ–T_e) curve of the machine at the steady-state operating point [10], i.e.,

$$k_e = \frac{\partial T_e}{\partial \delta}|_{\delta_0}. \tag{14}$$

《高階會員專屬-第31期》IEEE論文導讀：穩定的永磁同步電機Sensorless開回路VF控制技術

This simplified small-signal dynamics model and the power balance equation of the machine can be used to show how damping can be added to the system by modulating the applied frequency proportional to the perturbations of the input power of the machine.

The motor power balance equation can be written as

$$\begin{aligned} p_e =& P_e + \Delta p_e \\ =& p_{ml} + \frac{dw_{em}}{dt} + \left(\frac{2}{n}\right)^2 \frac{J}{2}\frac{d}{dt}\omega_r^2 + \left(\frac{2}{n}\right)^2 B_m \omega_r^2 + \frac{2}{n}\omega_r T_l \end{aligned} \tag{15}$$

where p_e is input power. P_e and Δp_e are the steady-state value and perturbation component of the input power, respectively. The input power is distributed among the motor losses p_{ml}, the

《高階會員專屬-第31期》IEEE論文導讀：穩定的永磁同步電機Sensorless開回路VF控制技術

change in electromagnetic energy storage w_{em}, and the mechanical output power of the machine. From (15), it can be seen that the rotor velocity perturbations should mainly contribute to generate the power perturbations for an operating point. Therefore, the power perturbations are approximated coming from rotor velocity perturbations of the last three terms of (15). With this approximation the perturbations in the power can be written as

$$\Delta p_e = \left(\frac{2}{n}\right)^2 J\omega_0 \frac{d}{dt}\Delta\omega_r + 2\left(\frac{2}{n}\right)^2 B_m\omega_0\Delta\omega_r + \frac{2}{n}T_{l0}\Delta\omega_r \tag{16}$$

where T_{l0} is the steady-state load torque. If the applied frequency is modulated proportionally to the power perturbations, then $\Delta\omega_e$ can be written as

《高階會員專屬-第31期》IEEE論文導讀：穩定的永磁同步電機Sensorless開回路VF控制技術

where T_{l0} is the steady-state load torque. If the applied frequency is modulated proportionally to the power perturbations, then $\Delta\omega_e$ can be written as

$$\Delta\omega_e = -k_p\Delta p_e = k_p\left[\left(\frac{2}{n}\right)^2 J\omega_0\frac{d}{dt}(-\Delta\omega_r) + 2\left(\frac{2}{n}\right)^2 B_m\omega_0(-\Delta\omega_r) + \frac{2}{n}T_{l0}(-\Delta\omega_r)\right] \quad (17)$$

where k_p is the proportional gain. With this type of modulation for the applied frequency, the simplified small-signal dynamics model given in Fig. 7 can be drawn as shown in Fig. 8.

《高階會員專屬-第31期》IEEE論文導讀：穩定的永磁同步電機Sensorless開回路VF控制技術

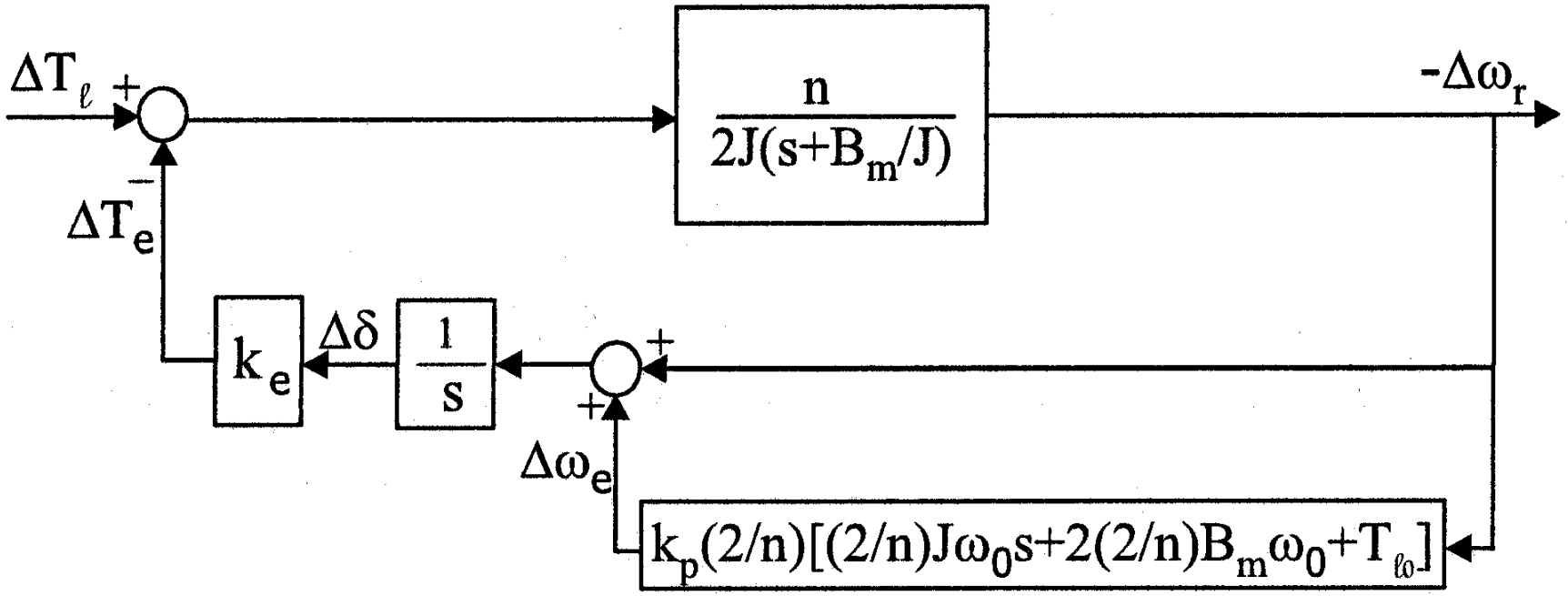

Fig. 8. Block diagram representation of the PMSM simplified small-signal dynamics when the applied frequency is modulated proportionally to the input power perturbations, i.e., $\Delta\omega_e = -k_p \Delta p_e$.

《高階會員專屬-第31期》IEEE論文導讀：穩定的永磁同步電機Sensorless開回路VF控制技術

The block diagram in Fig. 8 gives the characteristic equation for the system as

$$s^2 + \left(\frac{B_m}{J} + \frac{2k_e\omega_0 k_p}{n}\right) s + \frac{k_e}{2J}\left[n + \left(\frac{8}{n}\right) B_m k_p \omega_0 + 2T_{l0} k_p\right] = 0. \quad (18)$$

It can be seen from (18) that the damping of the system poles can be controlled by properly selecting the gain k_p. The root locus analysis made for the characteristic (18) shows that keeping the $\omega_0 k_p$ term constant, i.e., changing the k_p inversely proportional to the rotor speed, an almost constant damping factor (a constant real part for the system poles) can be obtained. This reveals that the location of the machine rotor poles in the s plane can be controlled using the gain k_p when the applied frequency is modulated according to (17).

0.064 s) and the gain for the stabilizing loop is calculated as $k_p = 8/\omega_0$ for $\omega_0 \neq 0$. Comparing Fig. 9 with Fig. 6, the added

《高階會員專屬-第31期》IEEE論文導讀：穩定的永磁同步電機Sensorless開回路VF控制技術

B. Stability Verification Using Full Small-Signal Dynamics Model

The simplified small-signal dynamics model, which has been used for the analysis in Section III-A, is an easy tool to predict how the applied frequency should be modulated to add damping to the system. However, the simplified small-signal dynamics

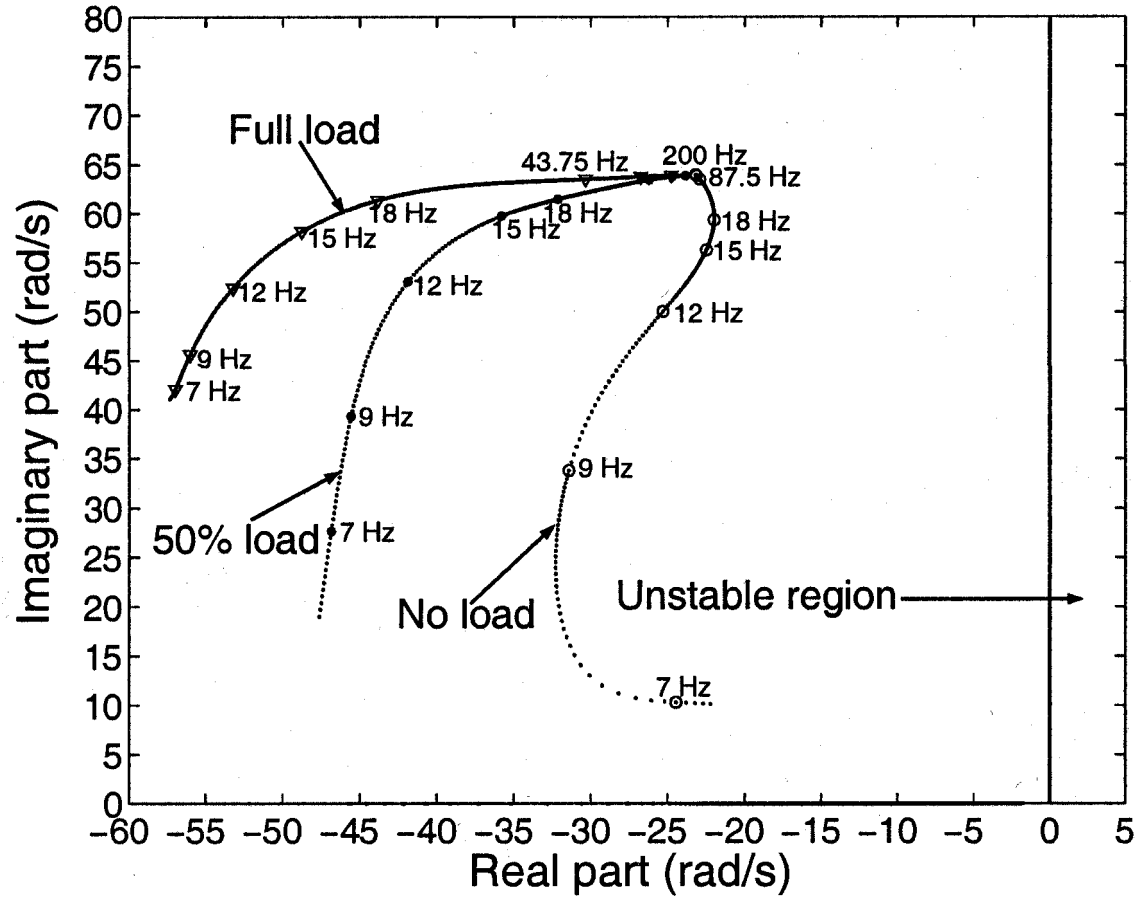

Fig. 9. Loci of the rotor poles under different load conditions, as a function of the applied frequency, with the frequency-modulated stabilizing loop in the system.

《高階會員專屬-第31期》IEEE論文導讀：穩定的永磁同步電機Sensorless開回路VF控制技術

C. Implementation of the Stabilizing Loop

To implement the stabilizing loop, the frequency modulation signal $\Delta\omega_e$ should be derived using the input power perturbations in the system as given in (19).

The input power to the machine is given by

$$p_e = \frac{3}{2} v_s i_s \cos\phi. \tag{27}$$

The $i_s \cos\phi$ term, which is used to calculate the voltage command in (6) and expressed in (4), and the commanded voltage reference to the machine v_s^* can be used in (27) to calculate the input power. As explained in Section III-B, a first-order high-pass filter can be used to extract the perturbations in the input power. With this knowledge, the derivation of the frequency modulation signal $\Delta\omega_e$ is shown in Fig. 10. The implementation of the full drive scheme with the stabilizing loop is shown in Fig. 11.

$$i_s \cos\phi = \frac{2}{3}\left[i_{as}\cos\theta_e + i_{bs}\cos\left(\theta_e - \frac{2\pi}{3}\right) - (i_{as}+i_{bs})\cos\left(\theta_e + \frac{2\pi}{3}\right)\right] \tag{4}$$

$$v_s^* = (i_s\cos\phi)r_s + \sqrt{(2\pi f_0 \lambda_m)^2 + (i_s\cos\phi)^2 r_s^2 - i_s^2 r_s^2}. \tag{6}$$

《高階會員專屬-第31期》IEEE論文導讀：穩定的永磁同步電機Sensorless開回路VF控制技術

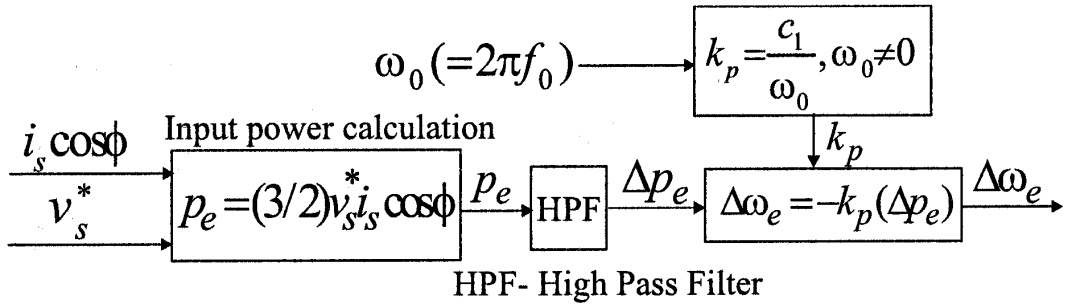

Fig. 10. Derivation of the frequency modulation signal $\Delta\omega_e$.

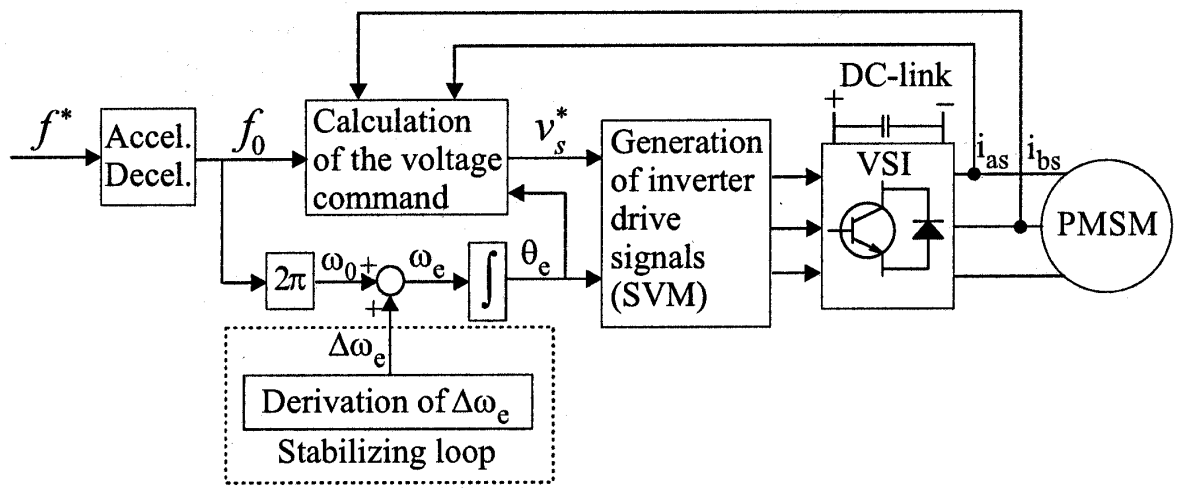

Fig. 11. Complete drive scheme with the stabilizing loop.

《高階會員專屬-第31期》IEEE論文導讀：穩定的永磁同步電機Sensorless開回路VF控制技術

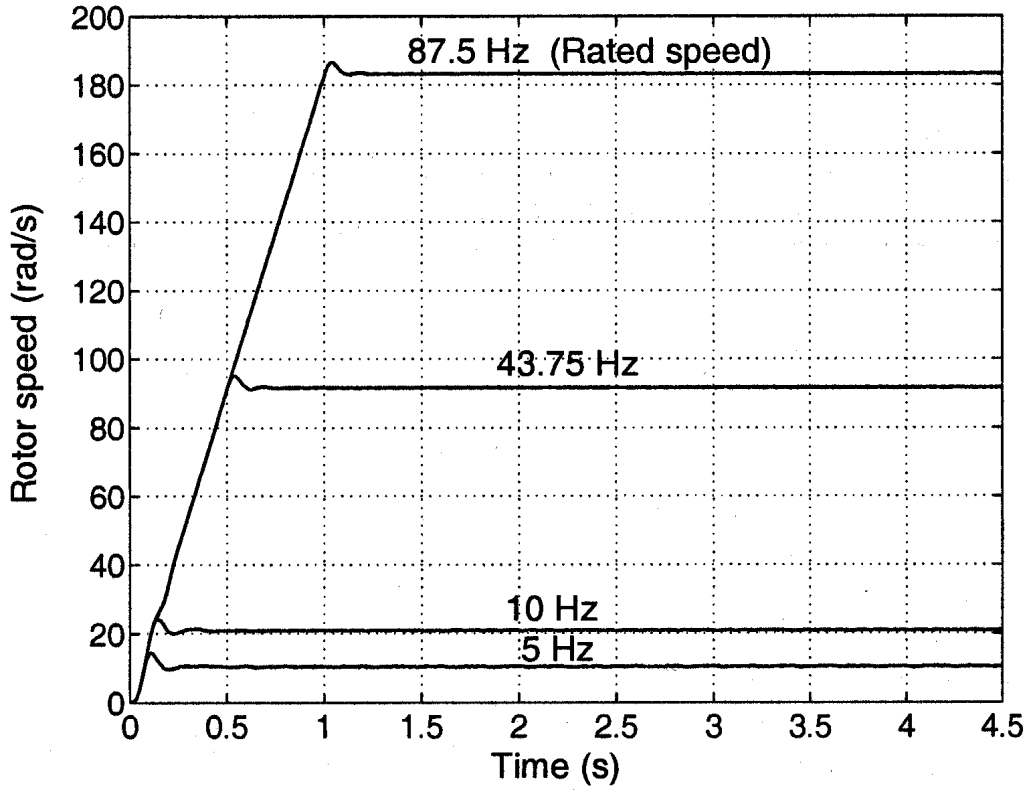

Fig. 14. Measured rotor speeds at different frequencies, under no load, with stabilizing loop in the system.

《高階會員專屬-第31期》IEEE論文導讀：穩定的永磁同步電機Sensorless開回路VF控制技術

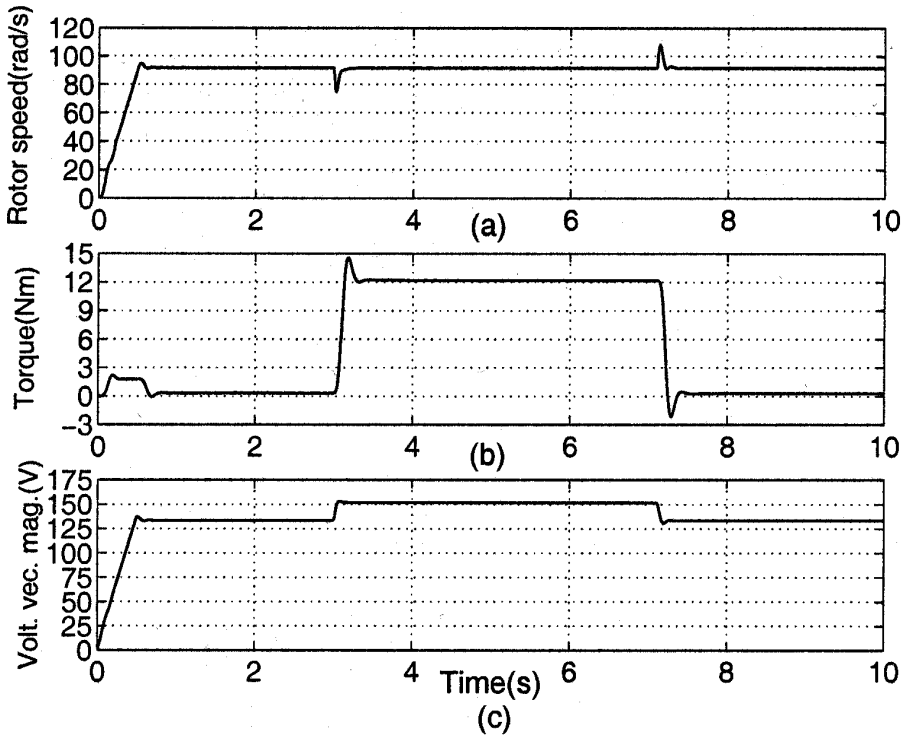

Fig. 15. Measured variables with a 100% load step to the drive at 50% of the rated speed. (a) Rotor speed. (b) Measured torque on the rotor shaft. (c) Commanded magnitude of the voltage vector.

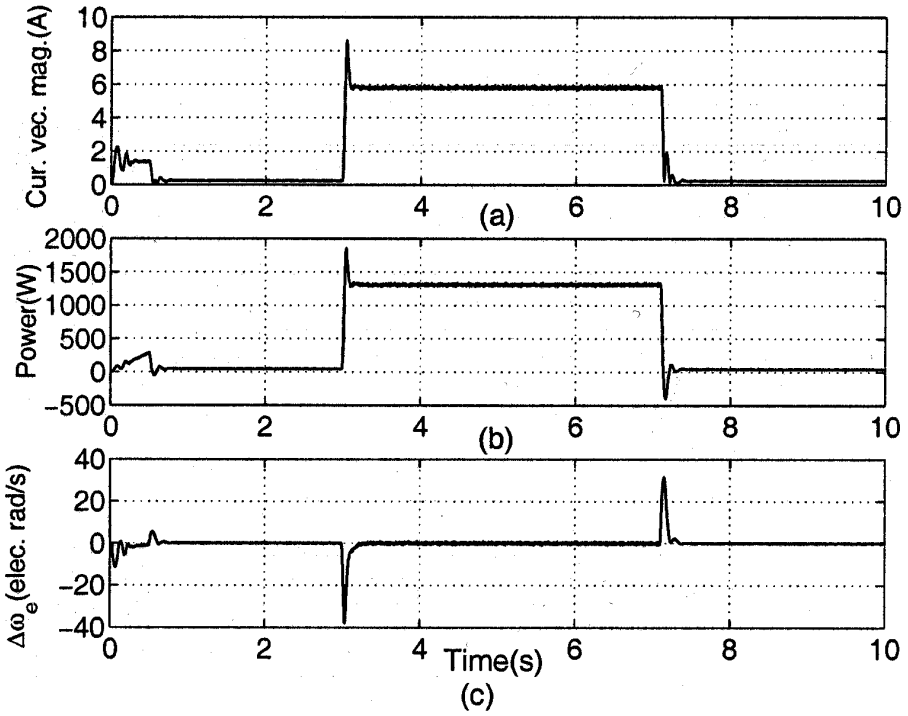

Fig. 16. Measured variables with a 100% load step to the drive at 50% of the rated speed. (a) Magnitude of the current vector. (b) Input power. (c) Frequency modulation signal $\Delta\omega_e$.

《高階會員專屬-第31期》IEEE論文導讀：穩定的永磁同步電機Sensorless開回路VF控制技術

The same test was carried out with the drive configuration shown in Fig. 11, i.e., with the stabilizing loop in the system. The stabilizing loop parameters which were used to calculate the eigenvalue plots in Fig. 9 were used in the drive system. Since the stable operation of the machine was possible at low frequencies the stabilizing loop was added to the system after exceeding the applied frequency of 3 Hz. Fig. 14 shows the results. Comparing Figs. 13 and 14, the effectiveness of the stabilizing loop in the system can be seen.

Figs. 15 and 16 show the measured variables from the proposed drive system with stabilizing loop, when adding a 12-N·m load step (100% load step) to the machine at 43.8 Hz (50% of the rated frequency). The results in these two figures indicate the drive's capability of overcoming a sudden load change in the system.

《高階會員專屬-第31期》IEEE論文導讀：穩定的永磁同步電機Sensorless開回路VF控制技術

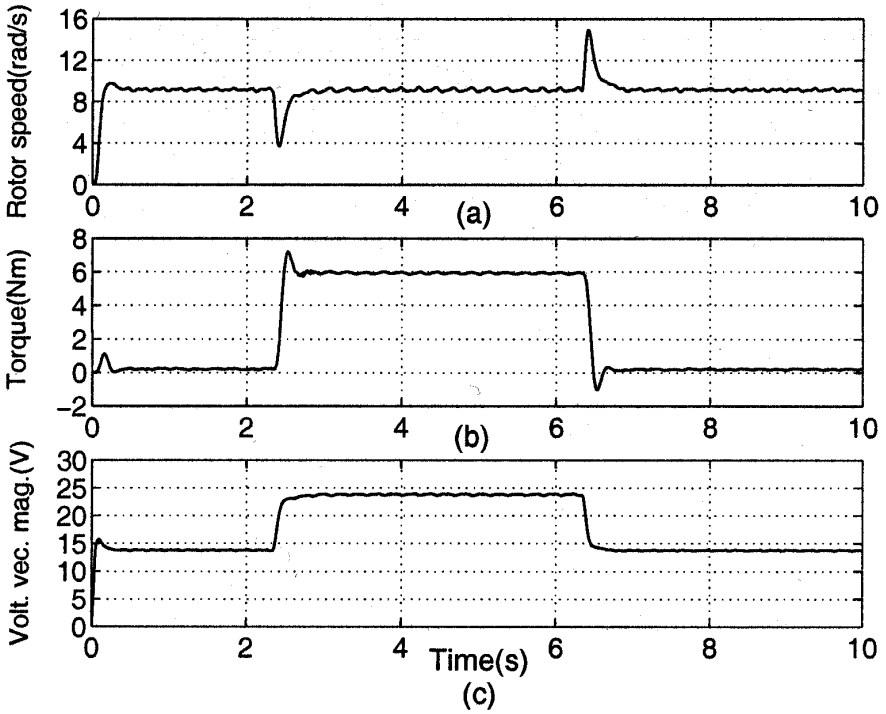

Fig. 17. Measured variables with a 50% load step to the drive at 5% of the rated speed. (a) Rotor speed. (b) Measured torque on the rotor shaft. (c) Commanded magnitude of the voltage vector.

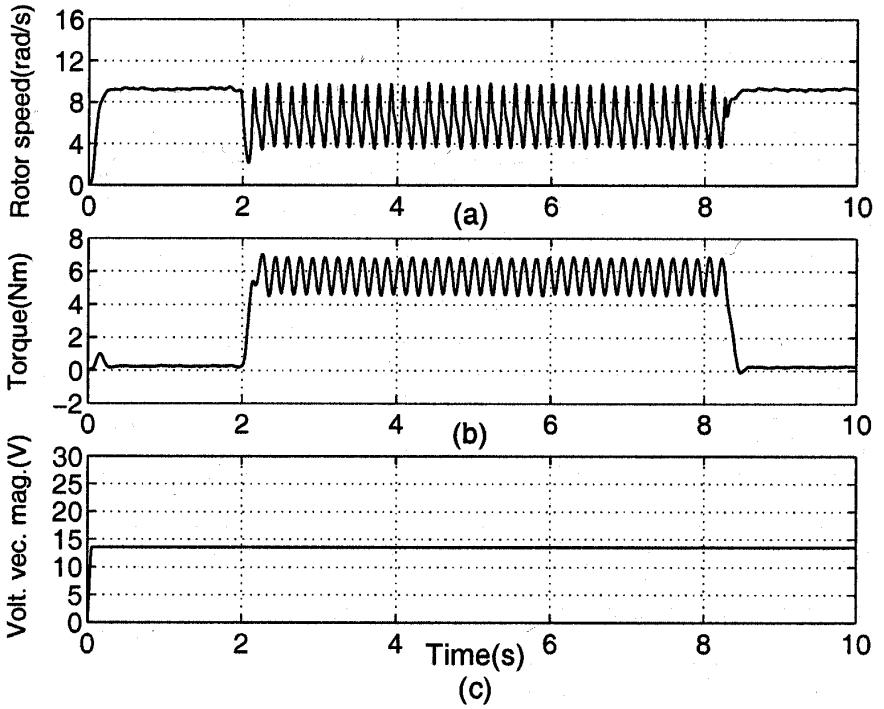

Fig. 18. Measured variables with a 50% load step at 5% of the rated speed, without r_s voltage drop compensation in voltage control of the drive. (a) Rotor speed. (b) Measured torque on the rotor shaft. (c) Commanded magnitude of the voltage vector.

《高階會員專屬-第31期》IEEE論文導讀：穩定的永磁同步電機Sensorless開回路VF控制技術

To verify the importance of the r_s voltage drop compensation (especially at low frequencies) in the voltage control of the machine, two tests were carried out. For the first test, the complete drive configuration shown in Fig. 11 was used, whereas for the second test only the voltage control of the drive was changed to the relationship given in (3), i.e., voltage control without r_s voltage drop compensation. Both tests were done at 4.4 Hz (5% of the rated frequency) with 50% load step. The measurements are shown in Figs. 17 and 18, respectively. It can be seen from Fig. 18 that the drive cannot overcome the load change due to the lack of voltage to the machine.

《高階會員專屬-第31期》IEEE論文導讀：穩定的永磁同步電機Sensorless開回路VF控制技術